Two-way Optimization for RIS Empowered FDD MIMO Communication Systems

Gyoseung Lee*, Hyeongtaek Lee*, A. Lee. Swindlehurst†, and Junil Choi*

*School of EE, Korea Advanced Institute of Science and Technology, Daejeon, South Korea
Email: {iee4432, htlee8459, junil}@kaist.ac.kr
†Department of EECS, University of California, Irvine, CA, USA
Email: swindle@uci.edu

2024 IEEE Wireless Communications and Networking Conference (WCNC) | 979-8-3503-0358-2/24/$31.00 ©2024 IEEE | DOI: 10.1109/WCNC57260.2024.10570791

***Abstract*—Due to the simultaneous downlink and uplink transmissions in reconfigurable intelligent surface (RIS)-empowered frequency division duplexing (FDD) communication systems, it is necessary to design the RIS phase shifts to balance the performance of both directions at the same time. Focusing on a single-user multiple-input multiple-output system, we aim to maximize a weighted sum-rate for the downlink and uplink. To address the resulting non-convex optimization problem, we employ an alternating optimization (AO) algorithm, which includes two techniques for optimizing the phase shifts at the RIS. A manifold optimization-based algorithm is applied for the first technique, and a lower-complexity AO approach is developed for the second. Our numerical results demonstrate that the proposed algorithms lead to substantial enhancement of the entire system compared to existing baseline schemes.**

I. Introduction

In recent years, reconfigurable intelligent surfaces (RISs) have drawn great interest for future wireless communication systems. An RIS can intelligently manipulate the characteristics of incoming signals, such as amplitude and phase, thereby leading to desired signal propagation [1]–[4].

Most of previous works related to RIS-empowered communication systems have assumed time division duplexing to take advantage of the reciprocal relationship between the downlink and uplink channels [5]–[9]. However, it is important to note that sub-6 GHz bands will still be frequently employed in future wireless communication systems due to their wide coverage and reliability [10], implying that the deployment of RISs in frequency division duplexing (FDD) systems would be inevitable.

In RIS-empowered FDD systems, an important characteristic is that the downlink and uplink signals are transmitted at the same time in separate frequency bands. Since the RIS lacks the capability for baseband processing, it affects signal reflection irrespective of the frequency band [11]. This implies that, as long as the difference between the downlink and uplink frequency bands is not extremely large, the same phase shifts are applied at the RIS for both the downlink and uplink transmissions. Consequently, in order to enhance the performance of both the downlink and uplink systems simultaneously, the optimization of RIS phase shifts should consider both directions, and some recent works have attempted to address this problem [12]–[14]. For single-user multiple-input single-output (SU-MISO) systems, two-way designs were developed in [12]. Furthermore, a practical RIS model was considered in [13] for SU-MISO systems. In [14], joint optimization strategies for multi-user MISO systems were developed. However, to the best of our knowledge, no prior work has addressed the two-way design for cases involving multi-antenna user equipment (UE) in FDD systems.

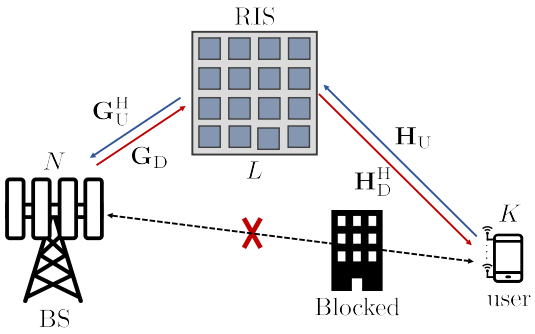

Fig. 1: An illustration of an RIS-empowered FDD SU-MIMO communication system. The BS and UE are equipped with N antennas and K antennas, and the RIS is composed of L passive elements.

In this paper, we aim to solve the weighted sum-rate maximization problem for the downlink and uplink in FDD single-user multiple-input multiple-output (SU-MIMO) systems. To tackle the problem, we develop two techniques to optimize the RIS reflection coefficients based on an alternating optimization (AO) approach. The first technique utilizes a manifold optimization-based algorithm, while for the second technique a lower complexity AO algorithm is developed. From the numerical results, we verify that the overall system performance can be substantially enhanced by the proposed joint optimization frameworks compared to existing baseline schemes.

II. System Model

We investigate an RIS-empowered FDD SU-MIMO system such as that illustrated in Fig. 1, where the base station (BS) with N antennas communicates with a single UE equipped with K antennas. A single RIS composed of L passive elements is also present, allowing the BS to achieve favorable signal propagation through a controller connected to the BS.

We assume that the channels between the BS and UE are entirely blocked, as in [7], [12].

In the downlink, the signal sent from the BS is expressed as $\mathbf{s}_{\mathrm{D}} \in \mathbb{C}^{N_{\mathrm{s}}^{\mathrm{D}} \times 1}$ with $\mathbb{E}\left[\mathbf{s}_{\mathrm{D}}\mathbf{s}_{\mathrm{D}}^{\mathrm{H}}\right] = \mathbf{I}_{N_{\mathrm{s}}^{\mathrm{D}}}$, where $N_{\mathrm{s}}^{\mathrm{D}} \leq \min(N, K)$ denotes the number of data streams from the BS. Then, the downlink received signal at the UE is represented by

$$\mathbf{y}_{\mathrm{D}} = \mathbf{H}_{\mathrm{D}}^{\mathrm{H}}\boldsymbol{\Theta}\mathbf{G}_{\mathrm{D}}\mathbf{F}_{\mathrm{D}}\mathbf{s}_{\mathrm{D}} + \mathbf{n}_{\mathrm{D}}, \tag{1}$$

where $\mathbf{F}_{\mathrm{D}} \in \mathbb{C}^{N \times N_{\mathrm{s}}^{\mathrm{D}}}$ is the downlink precoder at the BS satisfying $\mathrm{tr}(\mathbf{F}_{\mathrm{D}}\mathbf{F}_{\mathrm{D}}^{\mathrm{H}}) \leq P_{\mathrm{D,max}}$ with $P_{\mathrm{D,max}}$ representing maximum downlink transmit power at the BS, $\mathbf{H}_{\mathrm{D}}^{\mathrm{H}} \in \mathbb{C}^{K \times L}$ is the downlink channel between the RIS and the UE, $\mathbf{G}_{\mathrm{D}} \in \mathbb{C}^{L \times N}$ is the downlink channel between the BS and the RIS, and an additive white Gaussian noise (AWGN) vector at the UE is denoted by $\mathbf{n}_{\mathrm{D}} \sim \mathcal{CN}(\mathbf{0}_K, \sigma_{\mathrm{D}}^2\mathbf{I}_K)$ with noise variance σ_{D}^2. The matrix consisting of the reflection coefficients at the RIS is modeled as $\boldsymbol{\Theta} = \mathrm{diag}\left([\theta_1, \cdots, \theta_L]^{\mathrm{T}}\right)$ with $|\theta_\ell| = 1$, $\ell = 1, \cdots, L$.

In the uplink, the signal transmitted from the UE is expressed as $\mathbf{s}_{\mathrm{U}} \in \mathbb{C}^{N_{\mathrm{s}}^{\mathrm{U}} \times 1}$ with $\mathbb{E}\left[\mathbf{s}_{\mathrm{U}}\mathbf{s}_{\mathrm{U}}^{\mathrm{H}}\right] = \mathbf{I}_{N_{\mathrm{s}}^{\mathrm{U}}}$, where $N_{\mathrm{s}}^{\mathrm{U}} \leq \min(N, K)$ is the number of data streams from the UE. Note that the RIS is not able to execute local signal processing, and since the difference between the downlink and uplink carrier frequencies is assumed to not be too great [11], [12], the reflection coefficient matrix $\boldsymbol{\Theta}$ in (1) is also applied to the uplink transmission. The uplink received signal at the BS is therefore given by

$$\mathbf{y}_{\mathrm{U}} = \mathbf{G}_{\mathrm{U}}^{\mathrm{H}}\boldsymbol{\Theta}\mathbf{H}_{\mathrm{U}}\mathbf{F}_{\mathrm{U}}\mathbf{s}_{\mathrm{U}} + \mathbf{n}_{\mathrm{U}}, \tag{2}$$

where $\mathbf{F}_{\mathrm{U}} \in \mathbb{C}^{K \times N_{\mathrm{s}}^{\mathrm{U}}}$ is the uplink precoder at the UE satisfying $\mathrm{tr}(\mathbf{F}_{\mathrm{U}}\mathbf{F}_{\mathrm{U}}^{\mathrm{H}}) \leq P_{\mathrm{U,max}}$ with $P_{\mathrm{U,max}}$ representing maximum uplink transmit power at the UE, $\mathbf{G}_{\mathrm{U}}^{\mathrm{H}} \in \mathbb{C}^{N \times L}$ is the uplink channel between the RIS and the BS, $\mathbf{H}_{\mathrm{U}} \in \mathbb{C}^{L \times K}$ is the uplink channel between the UE and the RIS, and an AWGN vector at the BS is denoted by $\mathbf{n}_{\mathrm{U}} \sim \mathcal{CN}(\mathbf{0}_N, \sigma_{\mathrm{U}}^2\mathbf{I}_N)$ with noise variance σ_{U}^2.

The downlink and uplink achievable rates R_{D} and R_{U} can be represented by

$$\begin{aligned} R_{\mathrm{D}} &= \log_2 \det\left(\mathbf{I}_K + \frac{1}{\sigma_{\mathrm{D}}^2}\mathbf{H}_{\mathrm{eff,D}}\mathbf{F}_{\mathrm{D}}\mathbf{F}_{\mathrm{D}}^{\mathrm{H}}\mathbf{H}_{\mathrm{eff,D}}^{\mathrm{H}}\right) \\ R_{\mathrm{U}} &= \log_2 \det\left(\mathbf{I}_N + \frac{1}{\sigma_{\mathrm{U}}^2}\mathbf{H}_{\mathrm{eff,U}}\mathbf{F}_{\mathrm{U}}\mathbf{F}_{\mathrm{U}}^{\mathrm{H}}\mathbf{H}_{\mathrm{eff,U}}^{\mathrm{H}}\right), \end{aligned} \tag{3}$$

where $\mathbf{H}_{\mathrm{eff,D}} = \mathbf{H}_{\mathrm{D}}^{\mathrm{H}}\boldsymbol{\Theta}\mathbf{G}_{\mathrm{D}}$ and $\mathbf{H}_{\mathrm{eff,U}} = \mathbf{G}_{\mathrm{U}}^{\mathrm{H}}\boldsymbol{\Theta}\mathbf{H}_{\mathrm{U}}$ respectively denote the effective downlink and uplink channels.

III. Problem Setting and Algorithm Development

A. Problem formulation

Due to the simultaneous downlink and uplink transmissions in FDD, we aim to maximize the weighted sum-rate for the downlink and uplink as [12], [14]

$$\begin{aligned} (\mathrm{P1}): \max_{\mathbf{F}_{\mathrm{D}}, \mathbf{F}_{\mathrm{U}}, \boldsymbol{\Theta}} \quad & R_{\mathrm{WSR}} = \eta R_{\mathrm{D}} + (1-\eta)R_{\mathrm{U}} && (4) \\ \text{s.t.} \quad & \mathrm{tr}(\mathbf{F}_{\mathrm{D}}\mathbf{F}_{\mathrm{D}}^{\mathrm{H}}) \leq P_{\mathrm{D,max}}, && (5) \\ & \mathrm{tr}(\mathbf{F}_{\mathrm{U}}\mathbf{F}_{\mathrm{U}}^{\mathrm{H}}) \leq P_{\mathrm{U,max}}, && (6) \\ & \boldsymbol{\Theta} = \mathrm{diag}\left([\theta_1, \cdots, \theta_L]^{\mathrm{T}}\right), && (7) \\ & |\theta_\ell| = 1, \ \ \ell = 1, \cdots, L, && (8) \end{aligned}$$

where $\eta \in [0, 1]$ denotes a weight coefficient that allows for the adjustment of the relative importance of the downlink and uplink rates. To tackle this non-convex problem, we employ an AO-based approach. Specifically, we first decompose (P1) into distinct downlink and uplink sub-problems for a fixed $\boldsymbol{\Theta}$, and the optimal downlink and uplink precoders can be derived using eigenmode transmissions [15]. For fixed $\mathbf{F}_{\mathrm{D}}$ and $\mathbf{F}_{\mathrm{U}}$, we propose two techniques for optimizing $\boldsymbol{\Theta}$.

B. Precoder designs for given RIS phase shifts

For a given $\boldsymbol{\Theta}$, (P1) boils down to solving the downlink and uplink sub-problems separately. The downlink sub-problem for (P1) is

$$\begin{aligned} \max_{\mathbf{F}_{\mathrm{D}}} \quad & R_{\mathrm{D}} \\ \text{s.t.} \quad & \mathrm{tr}(\mathbf{F}_{\mathrm{D}}\mathbf{F}_{\mathrm{D}}^{\mathrm{H}}) \leq P_{\mathrm{D,max}}. \end{aligned} \tag{9}$$

Let $\mathbf{H}_{\mathrm{eff,D}} = \tilde{\mathbf{U}}_{\mathrm{D}}\tilde{\boldsymbol{\Sigma}}_{\mathrm{D}}\tilde{\mathbf{V}}_{\mathrm{D}}^{\mathrm{H}}$ represent the truncated singular value decomposition (SVD) of $\mathbf{H}_{\mathrm{eff,D}}$ where $\tilde{\mathbf{V}}_{\mathrm{D}} \in \mathbb{C}^{N \times N_{\mathrm{s}}^{\mathrm{D}}}$. Then, the optimal $\mathbf{F}_{\mathrm{D}}$ for this problem can be obtained by

$$\mathbf{F}_{\mathrm{D}}^{\star} = \tilde{\mathbf{V}}_{\mathrm{D}}\mathbf{P}_{\mathrm{D}}^{\frac{1}{2}}, \tag{10}$$

where $\mathbf{P}_{\mathrm{D}} = \mathrm{diag}\left(\left[p_{\mathrm{D},1}^{\star}, \cdots, p_{\mathrm{D},N_{\mathrm{s}}^{\mathrm{D}}}^{\star}\right]^{\mathrm{T}}\right)$ is the power allocation matrix. The optimal power level assigned to the i-th data stream, $p_{\mathrm{D},i}^{\star}$, is the result of the water-filling power allocation $p_{\mathrm{D},i}^{\star} = \max(1/p_{\mathrm{D},0} - \sigma_{\mathrm{D}}^2/[\tilde{\boldsymbol{\Sigma}}_{\mathrm{D}}]_{i,i}, 0)$ for $i = 1, \cdots, N_{\mathrm{s}}^{\mathrm{D}}$, where $p_{\mathrm{D},0}$ is set such that $\sum_{i=1}^{N_{\mathrm{s}}^{\mathrm{D}}} p_{\mathrm{D},i}^{\star} = P_{\mathrm{D,max}}$. The uplink sub-problem for (P1) can be similarly defined, and the optimal $\mathbf{F}_{\mathrm{U}}$ can be obtained by following the same procedure as in (10).

C. RIS phase shifts design for given precoders

For given $\mathbf{F}_{\mathrm{D}}$ and $\mathbf{F}_{\mathrm{U}}$, the optimization problem of (P1) with respect to $\boldsymbol{\Theta}$ is given by

$$\begin{aligned} (\mathrm{P2}): \max_{\boldsymbol{\Theta}} \quad & R_{\mathrm{WSR}} && (11) \\ \text{s.t.} \quad & \boldsymbol{\Theta} = \mathrm{diag}\left([\theta_1, \cdots, \theta_L]^{\mathrm{T}}\right), && (12) \\ & |\theta_\ell| = 1, \ \ \ell = 1, \cdots, L. && (13) \end{aligned}$$

Due to the unit-modulus constraints (13), which make the problem highly non-convex, obtaining the optimal solution for (P2) is not straightforward. In the following section, we develop two optimization techniques to handle this issue.

IV. Proposed RIS Phase Shifts Designs

In this section, we develop two optimization techniques to obtain a practical solution for (P2). The first is a manifold optimization-based algorithm, while the second employs a lower-complexity AO technique obtained by deriving a practical closed-form expression for each RIS phase shift.

A. Manifold optimization

To solve (P2), the main challenge is to tackle the unit-modulus constraints (13). Fortunately, using the fact that the constraints (13) form a complex circle manifold $\mathcal{M} = \{\boldsymbol{\theta} \in \mathbb{C}^L : |\theta_1| = \cdots = |\theta_L| = 1\}$ [16], we can obtain a practical solution for (P2) by employing the Riemannian conjugate gradient (RCG) algorithm, which is the generalized conjugate gradient method adapted to the Riemannian manifold space and guarantees to convergence to a stationary point [16].

To implement the RCG-based algorithm, the Euclidean gradient of objective function $R_{\mathrm{WSR}} = \eta\nabla_{\boldsymbol{\theta}} R_{\mathrm{D}} + (1-\eta)\nabla_{\boldsymbol{\theta}} R_{\mathrm{U}}$ is derived to obtain the Riemannian gradient of R_{WSR}. From here on, we focus on the computation of $\nabla_{\boldsymbol{\theta}} R_{\mathrm{D}} = \left[\frac{\partial R_{\mathrm{D}}}{\partial \theta_1}, \cdots, \frac{\partial R_{\mathrm{D}}}{\partial \theta_L}\right]^{\mathrm{T}}$, and $\nabla_{\boldsymbol{\theta}} R_{\mathrm{U}}$ can be computed in the same way. Applying the chain rule in [17], the derivative of R_{D} in terms of θ_ℓ can be expressed as

$$\begin{aligned}\frac{\partial R_{\mathrm{D}}}{\partial \theta_\ell} =& \operatorname{tr}\left(\nabla_{\mathbf{H}_{\mathrm{eff,D}}} R_{\mathrm{D}} \cdot \frac{\partial \mathbf{H}_{\mathrm{eff,D}}^{\mathrm{H}}}{\partial \theta_\ell^*}\right) \\ &+ \operatorname{tr}\left((\nabla_{\mathbf{H}_{\mathrm{eff,D}}} R_{\mathrm{D}})^{\mathrm{H}} \cdot \frac{\partial \mathbf{H}_{\mathrm{eff,D}}}{\partial \theta_\ell^*}\right). \end{aligned} \tag{14}$$

From the complex differentials, it is possible to treat θ_ℓ and θ_ℓ^* as independent variables [18], implying that $\frac{\partial \mathbf{H}_{\mathrm{eff,D}}}{\partial \theta_\ell^*} = 0$, and the second term in (14) becomes zero. In the following proposition, we first derive $\nabla_{\mathbf{H}_{\mathrm{eff,D}}} R_{\mathrm{D}}$.

Proposition 1. *The Euclidean gradient* $\nabla_{\mathbf{H}_{\mathrm{eff,D}}} R_{\mathrm{D}}$ *is*

$$\nabla_{\mathbf{H}_{\mathrm{eff,D}}} R_{\mathrm{D}} = \frac{1}{\ln 2 \cdot \sigma_{\mathrm{D}}^2} \mathbf{H}_{\mathrm{eff,D}} \mathbf{F}_{\mathrm{D}} \left(\mathbf{I}_{N_{\mathrm{s}}^{\mathrm{D}}} + \frac{1}{\sigma_{\mathrm{D}}^2} \mathbf{F}_{\mathrm{D}}^{\mathrm{H}} \mathbf{H}_{\mathrm{eff,D}}^{\mathrm{H}} \mathbf{H}_{\mathrm{eff,D}} \mathbf{F}_{\mathrm{D}}\right)^{-1} \mathbf{F}_{\mathrm{D}}^{\mathrm{H}}. \tag{15}$$

Proof. The proof is based on the arguments in [[17], Theorem 1 and Lemma 3]. □

Next, the derivative of $\mathbf{H}_{\mathrm{eff,D}}^{\mathrm{H}}$ in terms of θ_ℓ^* is given by

$$\frac{\partial \mathbf{H}_{\mathrm{eff,D}}^{\mathrm{H}}}{\partial \theta_\ell^*} = (\mathbf{h}'_{\mathrm{D},\ell} \otimes \mathbf{G}_{\mathrm{D}}(\ell,:))^{\mathrm{H}}, \tag{16}$$

where $\mathbf{h}'_{\mathrm{D},\ell}$ is the ℓ-th column of $\mathbf{H}_{\mathrm{D}}^{\mathrm{H}}$, $\mathbf{G}_{\mathrm{D}}(\ell,:)$ represents the ℓ-th row of $\mathbf{G}_{\mathrm{D}}$, and $\otimes$ denotes the Kronecker product. Defining the ℓ-th column of $\mathbf{G}_{\mathrm{U}}^{\mathrm{H}}$ as $\mathbf{g}'_{\mathrm{U},\ell}$, the derivative of R_{U} in terms of θ_ℓ can be computed by following (15) and (16).

The details of the RCG-based algorithm can be found in [7], [12], [16], and we describe the entire algorithm for obtaining the solution to (P1) in Algorithm 1. If the objective function (4) does not increase beyond the designed threshold ϵ, the algorithm terminates.

B. Low-Complexity AO

In this subsection, we develop a low-complexity AO technique to obtain a practical solution for (P2). Specifically, the sub-problem of (P2) with respect to each reflection coefficient is formulated, and a closed-form expression is derived for each sub-problem. By iteratively updating the reflection coefficients, (P2) can be effectively solved.

Algorithm 1 Proposed Algorithm for (P1) Based on Manifold Optimization

1: **Input:** $\mathbf{G}_{\mathrm{D}}, \mathbf{H}_{\mathrm{D}}, \mathbf{G}_{\mathrm{U}}, \mathbf{H}_{\mathrm{U}}, \sigma_{\mathrm{D}}, \sigma_{\mathrm{U}}$.
2: **Initialization:** Set $t = 0$, generate the initial $\boldsymbol{\theta}^{(0)}$, and compute $\mathbf{F}_{\mathrm{D}}^{(0)}$ and $\mathbf{F}_{\mathrm{U}}^{(0)}$ according to (10)
3: **repeat**
4: With fixed $\mathbf{F}_{\mathrm{D}}^{(t)}$ and $\mathbf{F}_{\mathrm{U}}^{(t)}$, compute $\boldsymbol{\theta}^{(t+1)}$ using the **RCG-based algorithm**
5: With fixed $\boldsymbol{\theta}^{(t+1)}$, compute $\mathbf{F}_{\mathrm{D}}^{(t+1)}$ and $\mathbf{F}_{\mathrm{U}}^{(t+1)}$ according to (10)
6: $t \leftarrow t+1$
7: **until** $\|R_{\mathrm{WSR}}^{(t+1)} - R_{\mathrm{WSR}}^{(t)}\|_2 \le \epsilon$
8: **Output:** $\boldsymbol{\theta}^\star = \boldsymbol{\theta}^{(t)}, \mathbf{F}_{\mathrm{D}}^\star = \mathbf{F}_{\mathrm{D}}^{(t)}, \mathbf{F}_{\mathrm{U}}^\star = \mathbf{F}_{\mathrm{U}}^{(t)}$

Following [6], the achievable rates R_{D} and R_{U} in (3) can be reformulated with respect to θ_ℓ. For example, R_{D} can be rewritten by

$$\begin{aligned} R_{\mathrm{D}} &= \log_2 \det\left(\mathbf{I}_K + \theta_\ell \mathbf{A}_{\mathrm{D},\ell}^{-1} \mathbf{B}_{\mathrm{D},\ell} + \theta_\ell^* \mathbf{A}_{\mathrm{D},\ell}^{-1} \mathbf{B}_{\mathrm{D},\ell}^{\mathrm{H}}\right) \\ &\quad + \log_2 \det(\mathbf{A}_{\mathrm{D},\ell}) \\ &\triangleq g_{\mathrm{D},\ell}(\theta_\ell) + \log_2 \det(\mathbf{A}_{\mathrm{D},\ell}), \end{aligned} \tag{17}$$

where $\mathbf{A}_{\mathrm{D},\ell} \in \mathbb{C}^{K\times K}$ and $\mathbf{B}_{\mathrm{D},\ell} \in \mathbb{C}^{K\times K}$ can be found in (18) and (19) at the top of the next page with given $\mathbf{G}'_{\mathrm{D}} = \mathbf{G}_{\mathrm{D}}\mathbf{F}_{\mathrm{D}} = [\mathbf{g}'_{\mathrm{D},1}, \cdots, \mathbf{g}'_{\mathrm{D},L}]^{\mathrm{H}} \in \mathbb{C}^{L\times N_{\mathrm{s}}^{\mathrm{D}}}$. Similarly, R_{U} can be rewritten as $R_{\mathrm{U}} = g_{\mathrm{U},\ell}(\theta_\ell) + \log_2 \det(\mathbf{A}_{\mathrm{U},\ell})$, where $\mathbf{A}_{\mathrm{U},\ell} \in \mathbb{C}^{N\times N}$ and $\mathbf{B}_{\mathrm{U},\ell} \in \mathbb{C}^{N\times N}$ can be defined as in (18) and (19) with given $\mathbf{H}'_{\mathrm{U}} = \mathbf{H}_{\mathrm{U}}\mathbf{F}_{\mathrm{U}} = [\mathbf{h}'_{\mathrm{U},1}, \cdots, \mathbf{h}'_{\mathrm{U},L}]^{\mathrm{H}} \in \mathbb{C}^{L\times N_{\mathrm{s}}^{\mathrm{U}}}$.

By removing the irrelevant terms with respect to θ_ℓ, the sub-problem of (P2) can be formulated as

$$(\mathrm{P3}): \max_{\theta_\ell} \; g_\ell(\theta_\ell) = \eta g_{\mathrm{D},\ell}(\theta_\ell) + (1-\eta) g_{\mathrm{U},\ell}(\theta_\ell) \tag{20}$$

$$\text{s.t.} \quad |\theta_\ell| = 1. \tag{21}$$

To derive the solution to (P3), we analyze properties related to the matrices $\mathbf{A}_{\mathrm{D},\ell}^{-1}\mathbf{B}_{\mathrm{D},\ell}$ and $\mathbf{A}_{\mathrm{U},\ell}^{-1}\mathbf{B}_{\mathrm{U},\ell}$ on which the objective function (20) depends. From (18) and (19), it is obvious that the rank of both $\mathbf{A}_{\mathrm{D},\ell}^{-1}\mathbf{B}_{\mathrm{D},\ell}$ and $\mathbf{A}_{\mathrm{U},\ell}^{-1}\mathbf{B}_{\mathrm{U},\ell}$ cannot exceed one since $\mathbf{B}_{\mathrm{D},\ell}$ and $\mathbf{B}_{\mathrm{U},\ell}$ are rank-one. If the rank of $\mathbf{A}_{\mathrm{D},\ell}^{-1}\mathbf{B}_{\mathrm{D},\ell}$ or $\mathbf{A}_{\mathrm{U},\ell}^{-1}\mathbf{B}_{\mathrm{U},\ell}$ is zero, the corresponding components of (20) become independent of θ_ℓ. In the following, we analyze the scenarios where both matrices are rank-one, and the solution depends on whether these matrices are diagonalizable or not. Note that identifying that $\mathbf{A}_{\mathrm{D},\ell}^{-1}\mathbf{B}_{\mathrm{D},\ell}$ and $\mathbf{A}_{\mathrm{U},\ell}^{-1}\mathbf{B}_{\mathrm{U},\ell}$ are diagonalizable is equivalent to showing that $\operatorname{tr}\left(\mathbf{A}_{\mathrm{D},\ell}^{-1}\mathbf{B}_{\mathrm{D},\ell}\right) \neq 0$ and $\operatorname{tr}\left(\mathbf{A}_{\mathrm{U},\ell}^{-1}\mathbf{B}_{\mathrm{U},\ell}\right) \neq 0$ [6].

1) Diagonalizable case: In this case, an eigenvalue decomposition can be applied to both matrices:

$$\begin{aligned} \mathbf{A}_{\mathrm{D},\ell}^{-1}\mathbf{B}_{\mathrm{D},\ell} &= \mathbf{U}_{\mathrm{D},\ell}\boldsymbol{\Lambda}_{\mathrm{D},\ell}\mathbf{U}_{\mathrm{D},\ell}^{-1} \\ \mathbf{A}_{\mathrm{U},\ell}^{-1}\mathbf{B}_{\mathrm{U},\ell} &= \mathbf{U}_{\mathrm{U},\ell}\boldsymbol{\Lambda}_{\mathrm{U},\ell}\mathbf{U}_{\mathrm{U},\ell}^{-1}, \end{aligned} \tag{22}$$

where $\boldsymbol{\Lambda}_{\mathrm{D},\ell} = \operatorname{diag}(\lambda_{\mathrm{D},\ell}, 0, \cdots, 0)$ and $\boldsymbol{\Lambda}_{\mathrm{U},\ell} = \operatorname{diag}(\lambda_{\mathrm{U},\ell}, 0, \cdots, 0)$, with sole non-zero eigenvalues $\lambda_{\mathrm{D},\ell}$ and $\lambda_{\mathrm{U},\ell}$, respectively. By defining the first rows of $\mathbf{C}_{\mathrm{D},\ell} = \mathbf{U}_{\mathrm{D},\ell}^{\mathrm{H}}\mathbf{A}_{\mathrm{D},\ell}\mathbf{U}_{\mathrm{D},\ell}$ and $\mathbf{C}_{\mathrm{U},\ell} = \mathbf{U}_{\mathrm{U},\ell}^{\mathrm{H}}\mathbf{A}_{\mathrm{U},\ell}\mathbf{U}_{\mathrm{U},\ell}$ as

$$\mathbf{A}_{\mathrm{D},\ell} = \mathbf{I}_K + \frac{1}{\sigma_{\mathrm{D}}^2}\left(\sum_{i=1,i\neq\ell}^{L}\theta_i \mathbf{h}'_{\mathrm{D},i}(\mathbf{g}'_{\mathrm{D},i})^{\mathrm{H}}\right)\left(\sum_{i=1,i\neq\ell}^{L}\theta_i \mathbf{h}'_{\mathrm{D},i}(\mathbf{g}'_{\mathrm{D},i})^{\mathrm{H}}\right)^{\mathrm{H}} + \frac{1}{\sigma_{\mathrm{D}}^2}\mathbf{h}'_{\mathrm{D},\ell}(\mathbf{g}'_{\mathrm{D},\ell})^{\mathrm{H}}\mathbf{g}'_{\mathrm{D},\ell}(\mathbf{h}'_{\mathrm{D},\ell})^{\mathrm{H}}, \tag{18}$$

$$\mathbf{B}_{\mathrm{D},\ell} = \frac{1}{\sigma_{\mathrm{D}}^2}\mathbf{h}'_{\mathrm{D},\ell}(\mathbf{g}'_{\mathrm{D},\ell})^{\mathrm{H}}\left(\sum_{i=1,i\neq\ell}^{L}\theta_i^* \mathbf{g}'_{\mathrm{D},i}(\mathbf{h}'_{\mathrm{D},i})^{\mathrm{H}}\right). \tag{19}$$

$(\mathbf{c}'_{\mathrm{D},\ell})^{\mathrm{T}}$ and $(\mathbf{c}'_{\mathrm{U},\ell})^{\mathrm{T}}$ and the first columns of $\mathbf{C}_{\mathrm{D},\ell}^{-1}$ and $\mathbf{C}_{\mathrm{U},\ell}^{-1}$ as $\mathbf{c}_{\mathrm{D},\ell}$ and $\mathbf{c}_{\mathrm{U},\ell}$, respectively, $g_{\mathrm{D},\ell}(\theta_\ell)$ and $g_{\mathrm{U},\ell}(\theta_\ell)$ can be reformulated as [6]

$$g_{\mathrm{D},\ell}(\theta_\ell) = \log_2(1+|\lambda_{\mathrm{D},\ell}|^2(1-c'_{\mathrm{D},\ell 1}c_{\mathrm{D},\ell 1}) + 2\mathrm{Re}(\theta_\ell\lambda_{\mathrm{D},\ell})) \tag{23}$$

$$g_{\mathrm{U},\ell}(\theta_\ell) = \log_2(1+|\lambda_{\mathrm{U},\ell}|^2(1-c'_{\mathrm{U},\ell 1}c_{\mathrm{U},\ell 1}) + 2\mathrm{Re}(\theta_\ell\lambda_{\mathrm{U},\ell})), \tag{24}$$

where $c'_{\mathrm{D},\ell 1}$ and $c_{\mathrm{D},\ell 1}$ represent the first entries of $(\mathbf{c}'_{\mathrm{D},\ell})^{\mathrm{T}}$ and $\mathbf{c}_{\mathrm{D},\ell}$, and $c'_{\mathrm{U},\ell 1}$ and $c_{\mathrm{U},\ell 1}$ represent the first entries of $(\mathbf{c}'_{\mathrm{U},\ell})^{\mathrm{T}}$ and $\mathbf{c}_{\mathrm{U},\ell}$, respectively.

For further investigation of (23) and (24), let $\rho_1(\mathbf{M}) \geq \cdots \geq \rho_n(\mathbf{M})$ be the ordered singular values of an arbitrary $n\times n$ complex matrix $\mathbf{M}$. The following lemma gives an upper bound for $|\lambda_{\mathrm{D},\ell}|$.

Lemma 1. *An upper bound for $|\lambda_{\mathrm{D},\ell}|$ is given by $\rho_1\left(\mathbf{A}_{\mathrm{D},\ell}^{-1}\right)\rho_1\left(\mathbf{B}_{\mathrm{D},\ell}\right)$.*

Proof. Because $\mathbf{A}_{\mathrm{D},\ell}^{-1}\mathbf{B}_{\mathrm{D},\ell}$ is rank-one, an upper bound for $|\lambda_{\mathrm{D},\ell}|$ can be represented by

$$\begin{aligned}|\lambda_{\mathrm{D},\ell}| &= \left|\mathrm{tr}\left(\mathbf{A}_{\mathrm{D},\ell}^{-1}\mathbf{B}_{\mathrm{D},\ell}\right)\right| \overset{(a)}{\leq} \sum_{k=1}^{K}\rho_k\left(\mathbf{A}_{\mathrm{D},\ell}^{-1}\right)\rho_k\left(\mathbf{B}_{\mathrm{D},\ell}\right)\\ &\overset{(b)}{=} \rho_1\left(\mathbf{A}_{\mathrm{D},\ell}^{-1}\right)\rho_1\left(\mathbf{B}_{\mathrm{D},\ell}\right),\end{aligned} \tag{25}$$

where (a) can be derived by Von Neumann's trace inequality [19], and (b) follows from $\mathbf{B}_{\mathrm{D},\ell}$ being rank-one. □

From (18), it is observed that $\mathbf{A}_{\mathrm{D},\ell}$ is a symmetric matrix, implying that $\rho_1\left(\mathbf{A}_{\mathrm{D},\ell}^{-1}\right)$ is equivalent to $\rho_K\left(\mathbf{A}_{\mathrm{D},\ell}\right)$. By using the following lemma, we can further simplify the upper bound of (25).

Lemma 2. *When $N_{\mathrm{s}}^{\mathrm{D}} < K-1$, $\rho_K\left(\mathbf{A}_{\mathrm{D},\ell}\right) = 1$.*

Proof. Denote $\mathbf{X}' = \mathbf{X}\mathbf{X}^{\mathrm{H}}$ and $\mathbf{Y}' = \mathbf{Y}\mathbf{Y}^{\mathrm{H}}$ where $\mathbf{X} = \sum_{i=1,i\neq\ell}^{L}\theta_i\mathbf{h}'_{\mathrm{D},i}(\mathbf{g}'_{\mathrm{D},i})^{\mathrm{H}}$ and $\mathbf{Y} = \mathbf{h}'_{\mathrm{D},\ell}(\mathbf{g}'_{\mathrm{D},\ell})^{\mathrm{H}}$, which form $\mathbf{A}_{\mathrm{D},\ell}$ in (18). To derive the tightest bound for $N_{\mathrm{s}}^{\mathrm{D}}$, we assume $\mathbf{X}'$ and $\mathbf{Y}'$ have maximum rank, i.e., $\mathrm{rank}\left(\mathbf{X}'\right) = N_{\mathrm{s}}^{\mathrm{D}}$ and $\mathrm{rank}\left(\mathbf{Y}'\right) = 1$.

Let $\lambda_1(\mathbf{M}) \geq \cdots \geq \lambda_n(\mathbf{M})$ be the ordered eigenvalues of an arbitrary $n\times n$ Hermitian matrix $\mathbf{M}$. By Weyl's inequality [20], an upper bound for $\lambda_K\left(\mathbf{X}'+\mathbf{Y}'\right)$ can be represented by

$$\lambda_K\left(\mathbf{X}'+\mathbf{Y}'\right) \leq \lambda_i\left(\mathbf{X}'\right) + \lambda_{K+1-i}\left(\mathbf{Y}'\right), \;\; i = 1,\cdots,K. \tag{26}$$

By taking $i = N_{\mathrm{s}}^{\mathrm{D}}+1$, the right-hand side of (26) becomes zero, implying $\lambda_K\left(\mathbf{X}'+\mathbf{Y}'\right) = 0$ since $\mathbf{X}'+\mathbf{Y}'$ is positive semi-definite. Hence, from (18) it is obvious that $\lambda_K\left(\mathbf{A}_{\mathrm{D},\ell}\right)$ is only affected by $\mathbf{I}_K$, i.e., $\lambda_K\left(\mathbf{A}_{\mathrm{D},\ell}\right) = 1$, resulting in $\rho_K\left(\mathbf{A}_{\mathrm{D},\ell}\right) = 1$, which finishes the proof. □

Based on Lemma 2, the upper bound for $|\lambda_{\mathrm{D},\ell}|$ can be reduced to $\rho_1\left(\mathbf{B}_{\mathrm{D},\ell}\right)$, and since $\mathbf{B}_{\mathrm{D},\ell}$ is rank-one, it can be shown that $\rho_1\left(\mathbf{B}_{\mathrm{D},\ell}\right) = \|\mathbf{B}_{\mathrm{D},\ell}\|_{\mathrm{F}}$. Similarly, when $N_{\mathrm{s}}^{\mathrm{U}} < N-1$, the upper bound for $|\lambda_{\mathrm{U},\ell}|$ is given by $\|\mathbf{B}_{\mathrm{U},\ell}\|_{\mathrm{F}}$.

Following (19), it is obvious that the gains of the RIS-related channels heavily affect the quantities $\|\mathbf{B}_{\mathrm{D},\ell}\|_{\mathrm{F}}$ and $\|\mathbf{B}_{\mathrm{U},\ell}\|_{\mathrm{F}}$. Note that the RIS deployment typically aims to expand signal coverage and provide support to users located at longer distances or with weaker signal strengths. Consequently, it is reasonable to assume that both $|\lambda_{\mathrm{D},\ell}|$ and $|\lambda_{\mathrm{U},\ell}|$ are sufficiently small, and we employ the following first-order Taylor approximation at (23) and (24); $\log(1+x) \approx x$ around $x = 0$. After applying the approximation and removing the irrelevant terms with respect to θ_ℓ, the following approximate version of (P3) results:

$$\begin{aligned}(\mathrm{P4}):\;\; &\max_{\theta_\ell}\; h_\ell(\theta_\ell) = \eta\mathrm{Re}(\theta_\ell\lambda_{\mathrm{D},\ell}) + (1-\eta)\mathrm{Re}(\theta_\ell\lambda_{\mathrm{U},\ell})\\ &\text{s.t.}\;\; |\theta_\ell| = 1.\end{aligned} \tag{27}$$

Finally, a closed-form solution to (P4) is obtained via the following proposition.

Proposition 2. *The closed-form solution to (P4) is given by*

$$\theta_\ell^\star = \exp(-j\arg(\phi_\ell)), \tag{28}$$

where ϕ_ℓ can be found in (31) at the top of the next page.

Proof. Using Euler's formula, $h_\ell(\theta_\ell)$ in (P4) can be reformulated as

$$\begin{aligned}h_\ell(\theta_\ell) &= \eta|\lambda_{\mathrm{D},\ell}|\cos(\arg(\theta_\ell)+\arg(\lambda_{\mathrm{D},\ell}))\\ &\quad + (1-\eta)|\lambda_{\mathrm{U},\ell}|\cos(\arg(\theta_\ell)+\arg(\lambda_{\mathrm{U},\ell}))\end{aligned} \tag{29}$$

$$= A\cos(\arg(\theta_\ell)+\phi_\ell). \tag{30}$$

An expression for $\tan(\phi_\ell)$ can be derived using the trigonometric identity $\cos(a+b) = \cos a\cos b - \sin a\sin b$ in (29) and (30), and it is straightforward to show that ϕ_ℓ is equivalent to (31). Therefore, (30) is maximized when θ_ℓ is given as (28), which finishes the proof. □

2) Non-diagonalizable cases: According to [6], it can be shown that non-diagonalizable $\mathbf{A}_{\mathrm{D},\ell}^{-1}\mathbf{B}_{\mathrm{D},\ell}$ or $\mathbf{A}_{\mathrm{U},\ell}^{-1}\mathbf{B}_{\mathrm{U},\ell}$ makes $g_{\mathrm{D},\ell}(\theta_\ell)$ or $g_{\mathrm{U},\ell}(\theta_\ell)$ irrelevant to θ_ℓ. Hence, the solution in this case can be simply derived by maximizing the diagonalizable part, i.e., the solution is given by $\theta_\ell^\star = \exp(-j\arg(\lambda_{\mathrm{U},\ell}))$ or $\exp(-j\arg(\lambda_{\mathrm{D},\ell}))$. When both matrices are non-diagonalizable, there are infinitely many solutions, and we can set $\theta_\ell^\star = 1$ for simplicity.

$$\phi_\ell = \tan^{-1}\left(\frac{\eta|\lambda_{\mathrm{D},\ell}|\sin(\arg(\lambda_{\mathrm{D},\ell})) + (1-\eta)|\lambda_{\mathrm{U},\ell}|\sin(\arg(\lambda_{\mathrm{U},\ell}))}{\eta|\lambda_{\mathrm{D},\ell}|\cos(\arg(\lambda_{\mathrm{D},\ell})) + (1-\eta)|\lambda_{\mathrm{U},\ell}|\cos(\arg(\lambda_{\mathrm{U},\ell}))}\right), \tag{31}$$

3) Summary: Throughout this subsection, the closed-form expression for each sub-problem of (P2) is derived depending on the properties of $\mathbf{A}_{\mathrm{D},\ell}^{-1}\mathbf{B}_{\mathrm{D},\ell}$ and $\mathbf{A}_{\mathrm{U},\ell}^{-1}\mathbf{B}_{\mathrm{U},\ell}$. The entire low-complexity AO-based algorithm can be implemented by replacing the RCG-based algorithm in Algorithm 1 with the derived closed-form expressions, from which the reflection coefficients are updated sequentially. We omit a formal algorithm description due to the space limitations.

C. Complexity analysis

For the comparison of complexity between the two proposed algorithms, we assume $(N_{\mathrm{s}}^{\mathrm{D}}, N_{\mathrm{s}}^{\mathrm{U}}) \ll (N, K) \leq L$. First, the complexity of the manifold optimization-based algorithm is dominated by computation of the Euclidean gradient $\nabla_{\boldsymbol{\theta}} R_{\mathrm{WSR}}$, and the overall complexity is given by $\mathcal{O}(I_{\mathrm{out},1} I_{\mathrm{in}}(N^2KL + NK^2L))$, where $I_{\mathrm{out},1}$ and I_{in} are the number of outer and inner iterations for implementing the RCG-based algorithm, respectively. For the low-complexity AO-based algorithm, the complexity level can be demonstrated to be $\mathcal{O}(I_{\mathrm{out},2}(3(N^3 + K^3) + 2NK(N+K))L)$ assuming $I_{\mathrm{out},2}$ outer iterations. When $N = K$, the complexity of the two algorithms reduces to $\mathcal{O}(I_{\mathrm{out},1} I_{\mathrm{in}} N^3 L)$ and $\mathcal{O}(I_{\mathrm{out},2} N^3 L)$, respectively. This implies that the manifold optimization-based algorithm has higher complexity than the low-complexity AO approach due to the extra I_{in} term.

V. Numerical Results

In this section, we evaluate the performance of the proposed algorithms. For the simulations, the carrier frequencies for the downlink and uplink transmissions are set to be $f_{\mathrm{D}} = 2.135$ GHz and $f_{\mathrm{U}} = 1.945$ GHz. Both the BS and UE are assumed to have a uniform linear array equipped with $N = 14$ and $K = 6$ antennas, respectively. The RIS consists of a uniform planar array with L_{h} horizontal elements and L_{v} vertical elements. We set the locations of the BS, RIS, and UE as (0 m, 0 m), (800 m, 5 m), and (850 m, 0 m), respectively. The noise variance is $\sigma_{\mathrm{D}}^2 = \sigma_{\mathrm{U}}^2 =$ -104 dBm with noise spectral density -174 dBm/Hz and bandwidth 10 MHz. The weight coefficient is set to be $\eta = 0.5$, and the number of data streams is $N_{\mathrm{s}}^{\mathrm{D}} = N_{\mathrm{s}}^{\mathrm{U}} = 5$. The threshold to determine convergence of the proposed algorithms is set to be $\epsilon = 10^{-5}$.

We adopt the distance and frequency dependent path-loss model from 3GPP [14], [21] given by

$$\mathrm{PL}\,(d, f)\ \ [\mathrm{dB}] = 28 + 22\log_{10}\left(\frac{d}{d_0}\right) + 20\log_{10}\left(\frac{f}{f_0}\right), \tag{32}$$

where d denotes the link distance, f represent the carrier frequency, and the reference distance and frequency are given by $d_0 = 1$ m and $f_0 = 1$ GHz, respectively.

The one-way AO algorithm from [6] and the truncated-SVD-based-beamforming (T-SVD-BF) approach of [7] are used as baselines for performance comparison. The one-way AO approach corresponds to the case of $\eta = 1$ or 0 in the low-complexity AO algorithm discussed in Section IV-B. Therefore, in this scheme the reflection coefficients at the RIS are optimized only for the downlink or uplink. In T-SVD-BF, the singular values of the downlink and uplink effective channels, $\mathbf{H}_{\mathrm{eff,D}}$ and $\mathbf{H}_{\mathrm{eff,U}}$, are approximated with respect to the reflection coefficients, and the manifold optimization is employed to optimize the reflection coefficients. Note that in this scheme the reflection coefficients are optimized considering both the downlink and uplink. For all baseline schemes, the precoders at the BS and UE are updated based on eigenmode transmissions as discussed in Section III-B.

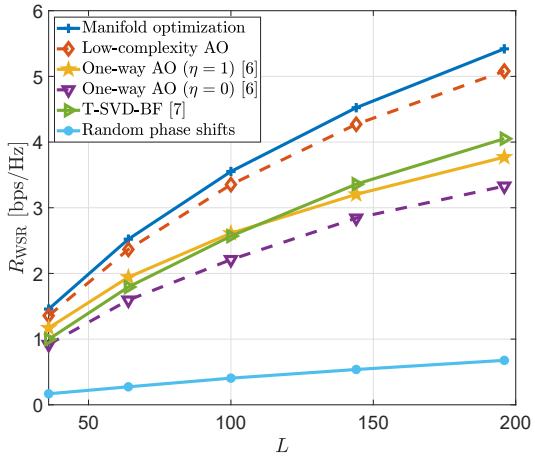

Fig. 2: Comparison of weighted sum-rate according to the number of RIS elements.

In Fig. 2, we investigate the weighted sum-rate according to the number of RIS elements L where $L_{\mathrm{h}} = L_{\mathrm{v}}$ assuming $P_{\mathrm{D,max}} = 28$ dBm and $P_{\mathrm{U,max}} = 23$ dBm. Regardless of the value of L, the two proposed algorithms lead to the highest weighted sum-rates, which demonstrates the importance of two-way design in FDD systems. Note that jointly optimized reflection coefficients in the manifold optimization-based algorithm result in a superior performance than the low-complexity AO-based algorithm. Nevertheless, for small L, the approximation applied in the low-complexity AO case is more accurate due the reduced channel gains, and thus its performance of relative to the manifold optimization-based algorithm is similar. It is observed that when L is small, T-SVD-BF shows lower weighted sum-rate than the one-way AO with $\eta = 1$. This is because the approximation for the singular values used in T-SVD-BF does not work well for small L. However, as L increases, T-SVD-BF shows superior performance than the one-way AO, which in turn enhances the efficiency of the joint optimization for the downlink and uplink.

In Fig. 3, we compare the weighted sum-rate according to

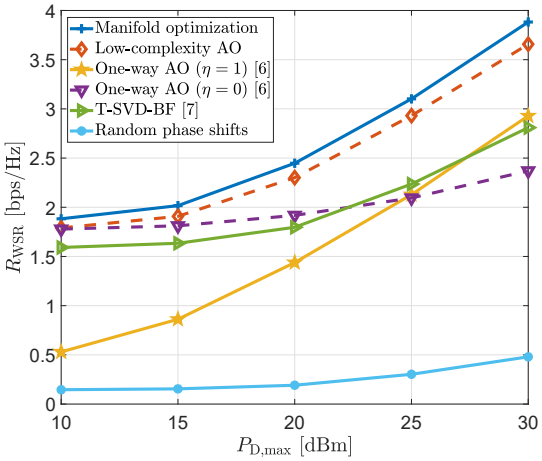

Fig. 3: Comparison of weighted sum-rate according to the downlink transmit power.

$P_{\mathrm{D,max}}$ for $P_{\mathrm{U,max}} = 23$ dBm and $L = 100$ with $L_{\mathrm{h}} = L_{\mathrm{v}} = 10$. Similar to the previous results, the proposed algorithms achieve the highest weighted sum-rates irrespective of the specific value of $P_{\mathrm{D,max}}$, which verifies their adaptability and effectiveness. The small performance gap between the one-way AO with $\eta = 0$ and the proposed algorithms when $P_{\mathrm{D,max}}$ is small reveals that it would be better to optimize the reflection coefficients only for the uplink when the downlink transmit power is limited. Likewise, the weighted sum-rate for the one-way AO with $\eta = 1$ improves dramatically with increasing $P_{\mathrm{D,max}}$. Still, the proposed algorithms outperform other baseline schemes for all practical ranges of $P_{\mathrm{D,max}}$.

VI. Conclusion

We proposed a joint optimization framework in RIS-empowered FDD SU-MIMO systems to maximize the downlink and uplink rates at the same time. To address the non-convex weighted sum-rate optimization problem, we first separated the precoder design from the reflection coefficient design, and the precoders are updated based on eigenmode transmission. For optimizing the reflection coefficients, a manifold optimization-based technique and a lower-complexity AO approach are developed. Our numerical results demonstrate that the proposed algorithms outperform existing baseline schemes.

Acknowledgement

This work was supported in part by LG Electronics Inc., by Basic Science Research Program through the National Research Foundation of Korea (NRF) funded by the Ministry of Education (RS-2023-00271715), by the Ministry of Science and ICT (MSIT), South Korea, under the Information Technology Research Center (ITRC) Support Program supervised by the Institute of Information and Communications Technology Planning and Evaluation (IITP) under Grant IITP-2020-0-01787, by the Korea Institute for Advancement of Technology (KIAT) grant funded by the Ministry of Trade, Industry and Energy (MOTIE) (P0022557), and by the U.S. National Science Foundation under grants CNS-2107182 and ECCS-2030029.

References

[1] Q. Wu and R. Zhang, "Towards Smart and Reconfigurable Environment: Intelligent Reflecting Surface Aided Wireless Network," *IEEE Commun. Mag.*, vol. 58, no. 1, pp. 106–112, Jan. 2020.

[2] M. Di Renzo *et al.*, "Smart Radio Environments Empowered by Reconfigurable AI Meta-Surfaces: An Idea Whose Time Has Come," *EURASIP J. Wirel. Commun. Netw.*, vol. 2019, no. 1, pp. 1–20, May 2019.

[3] E. Basar, M. Di Renzo, J. De Rosny, M. Debbah, M.-S. Alouini, and R. Zhang, "Wireless Communications Through Reconfigurable Intelligent Surfaces," *IEEE Access*, vol. 7, pp. 116 753–116 773, Aug. 2019.

[4] M. Di Renzo, F. H. Danufane, and S. Tretyakov, "Communication Models for Reconfigurable Intelligent Surfaces: From Surface Electromagnetics to Wireless Networks Optimization," *Proc. IEEE*, vol. 110, no. 9, pp. 1164–1209, Sep. 2022.

[5] C. Pan, H. Ren, K. Wang, J. F. Kolb, M. Elkashlan, M. Chen, M. Di Renzo, Y. Hao, J. Wang, A. L. Swindlehurst, X. You, and L. Hanzo, "Reconfigurable Intelligent Surfaces for 6G Systems: Principles, Applications, and Research Directions," *IEEE Commun. Mag.*, vol. 59, no. 6, pp. 14–20, Jun. 2021.

[6] S. Zhang and R. Zhang, "Capacity Characterization for Intelligent Reflecting Surface Aided MIMO Communication," *IEEE J. Sel. Areas Commun.*, vol. 38, no. 8, pp. 1823–1838, Jun. 2020.

[7] P. Wang, J. Fang, L. Dai, and H. Li, "Joint Transceiver and Large Intelligent Surface Design for Massive MIMO mmWave Systems," *IEEE Trans. Wirel. Commun.*, vol. 20, no. 2, pp. 1052–1064, Oct. 2021.

[8] S. H. Hong, J. Park, S.-J. Kim, and J. Choi, "Hybrid Beamforming for Intelligent Reflecting Surface Aided Millimeter Wave MIMO Systems," *IEEE Trans. Wirel. Commun.*, vol. 21, no. 9, pp. 7343–7357, Mar. 2022.

[9] S. Kim, H. Lee, J. Cha, S.-J. Kim, J. Park, and J. Choi, "Practical Channel Estimation and Phase Shift Design for Intelligent Reflecting Surface Empowered MIMO Systems," *IEEE Trans. Wirel. Commun.*, vol. 21, no. 8, pp. 6226–6241, Aug. 2022.

[10] H. Viswanathan and P. E. Mogensen, "Communications in the 6G Era," *IEEE Access*, vol. 8, pp. 57 063–57 074, Mar. 2020.

[11] Y. Chen, D. Chen, and T. Jiang, "Beam-Squint Mitigating in Reconfigurable Intelligent Surface Aided Wideband MmWave Communications," in *Proc. IEEE Wirel. Commun. Netw. Conf. (WCNC)*, Mar. 2021.

[12] B. Guo, C. Sun, and M. Tao, "Two-Way Passive Beamforming Design for RIS-Aided FDD Communication Systems," in *Proc. IEEE Wirel. Commun. Netw. Conf. (WCNC)*, May 2021.

[13] H. Zhou, Y.-C. Liang, R. Long, L. Zhao, and Y. Pei, "Reconfigurable Intelligent Surface for FDD Systems: Design and Optimization," *IEEE Internet Things J.*, vol. 10, no. 11, pp. 9607–9621, Jun. 2023.

[14] M. S. Abouamer and P. Mitran, "Joint Uplink-Downlink Resource Allocation for Multiuser IRS-Assisted Systems," *IEEE Trans. Wirel. Commun.*, vol. 21, no. 12, pp. 10 918–10 933, Jul. 2022.

[15] D. Tse and P. Viswanath, *Fundamentals of Wireless Communication*. Cambridge University Press, 2005.

[16] P.-A. Absil, R. Mahony, and R. Sepulchre, *Optimization Algorithms on Matrix Manifolds*. Princeton University Press, 2009.

[17] D. Palomar and S. Verdu, "Gradient of Mutual Information in Linear Vector Gaussian Channels," *IEEE Trans. Inf. Theory*, vol. 52, no. 1, pp. 141–154, Dec. 2006.

[18] A. Hjorungnes and D. Gesbert, "Complex-Valued Matrix Differentiation: Techniques and Key Results," *IEEE Trans. Signal Process.*, vol. 55, no. 6, pp. 2740–2746, May 2007.

[19] M. Carlsson, "Von Neumann's Trace Inequality for Hilbert–Schmidt Operators," *Expo. Math.*, vol. 39, no. 1, pp. 149–157, Mar. 2021.

[20] R. A. Horn and C. R. Johnson, *Matrix Analysis*. Cambridge University Press, 2012.

[21] *Evolved Universal Terrestiral Radio Access (E-UTRA); Radio Resource Control (RRC); Protocol Specification*. Document TS 38.901, Version 16.1.0, 3GPP, Mar. 2017.